Surge prevention for gas turbines connected with large volume size: experimental demonstration with a microturbine

M.L. Ferrari, P. Silvestri, F. Reggio, A.F. Massardo
Thermochemical Power Group (TPG)
University of Genoa, Italy

Contact author: Mario L. Ferrari (mario.ferrari@unige.it)

Abstract

The aim of this work is the demonstration of a surge prevention technique for advanced gas turbine cycles. There is significant surge risk in dynamic operation for turbines connected with large volume size additional components, such as a fuel cell stack, a saturator, a solar receiver or a heat exchanger for external combustion. In comparison with standard gas turbines, the volume size generates different behaviour during dynamic operations (with significant surge risk), especially considering that such additional components are including important dynamic constraints.

In order to prevent the surge events, a vibration analysis was carried out to develop precursors which are able to highlight the approach of this unstable operative zone. Since the sub-synchronous content of the measured vibrations is significantly increasing approaching the surge line, special attention was devoted to this parameter.

The demonstration of a surge prevention system based on the sub-synchronous vibration content was carried out at the Innovative Energy Systems Laboratory of the University of Genoa. In this laboratory, a recuperated microturbine connected with a large size vessel was used. Starting from the stable operation, closing a valve in the main air line or increasing the compressor inlet temperature produced operative conditions with significant surge risk. The increase in sub-

synchronous vibration content detected by the control system was used to perform an active operation (bleed valve opening) to avoid the approaching surge event.

Keywords

Large volume; Gas turbine; Dynamic operation; Surge prevention; Sub-synchronous vibrations.

1. Introduction

The global increase in energy demand and concerns regarding environmental conservation has led to the significant research in efficient power generation technologies (gas turbine aspects highlighted in: [1] for advanced cycles, [2] for high efficiency generation, [3] for thermoeconomic impact and [4] for applications in polygeneration grids) . However, remarkable efficiency increase is hard to achieve through further optimization of simple gas turbine cycle, since the existing technology is now close to its maximum improvement [5]. For this reason, advanced cycles based on the additional components can play a significant role to achieve the target of more efficient power generation [1]. Although these modified layouts are limited by cost and geometric constraints [6], different advanced cycles have reached the commercial level in specific fields [7]. A typical example includes the recuperated microturbine cycles which have acceptable efficiency in small size units [8]. Moreover, the significant research activities on concentrated solar power [9], micro Humid Air Turbine (micro-HAT) systems ([10] includes calculations on an entire micro-HAT plant and [11] an experimental campaign on the saturator, that is the most critical component), and fuel cell based hybrid plants [12] have shown a significant potential interest for gas turbines connected with additional components. An important aspect to be considered when additional components are included in the turbine cycle is the increased volume size in the zone located between the compressor outlet duct and the expander inlet. Although in some cases (e.g. recuperated cycle) the additional volume is just related to the additional ducts, several advanced configurations (e.g. the

mentioned hybrid systems) involve the additional volume which is more than two or three order of magnitudes larger than the standard machine one [13].

Even if the additional volume has not a significant impact on the steady-state performance, delayed response in the pressurization/depressurization phases during the transient operations results in a completely different behaviour. This aspect is critical for the plant constraints and control system. Thus, in order to consider this transient effect, standard controllers developed by the turbine manufacturers require a complete re-design activity. For instance, the standard shutdown phase has to be modified: implementing actions (on the fuel system or on the generator) to reduce the rotational speed decay and, hence, to avoid the surge conditions which are caused by the slow depressurization rate (in comparison with the standard machine behaviour) [14].

Among different kinds of risks which can be produced by the additional volume during transient operations, surge event is the most dangerous one for both the turbine and the connected components. For this reason, special attention is devoted to control techniques which are able to prevent such critical phenomenon [15]. Since compressor maps (when available) are not reliable to prevent surge [16] during all the operative conditions (e.g. in case of component degradation [17]), the definition of surge measurable precursors is mandatory for a wide commercialization of such advanced turbine-based plants.

Although some authors ([18] shows a statistical approach based on pressure measurements and [19] presents a vibration analysis on a compressor) have already presented possible surge precursors, the novelty of this paper regards the development of a gas turbine control approach that, on the basis of standard accelerometer measurements, is able to prevent surge events in case of critical conditions. The analysis is not focused on the fluid dynamic aspects of the machine components, but it is devoted to the entire cycle considering specific behaviour due to the additional volume [20]. Although the surge prevention method shown in this work has a general target for all the innovative gas turbines, the experimental work of this paper regards a T100 microturbine [21]. The selection of T100 microturbine for experimental investigation is motivated by the interest in

such plants for distributed generation [22], and due to the availability of a flexible rig [23] which includes a T100 microturbine coupled with a large size external volume.

The experiential demonstration shown in this paper was carried out with a flexible experimental facility which has been developed in previous works ([13] for a general rig presentation, [21] for the emulation technique based on a cyber-physical approach, [23] for the performance curves of the emulated system) by the Thermochemical Power Group (TPG) at the Innovative Energy Systems Laboratory - University of Genoa. Although this test rig was designed and installed for the emulation of Solid Oxide Fuel Cell (SOFC) hybrid systems [24], this plant can be used effectively for analysing the general impact of the volume size on the machine stability. The plant control system was equipped with an additional subroutine, which is able to calculate the sub-synchronous vibration content (the root mean square value) and to detect the significant value increases [25] in comparison with standard operations. Thus, producing an operative condition close to the surge zone ([26] and [27] show an experimental and numerical investigation related to surge events), the increase of this parameter was used as an indicator to perform the active operation (opening of the emergency bleed valve), and thus avoiding any instability risk.

This paper shows an innovative technique for surge prevention in advanced turbine-based plants. This will be an important solution to enlarge the application and the flexibility of these plants or to solve one of the major technical issues that are delaying commercial applications. The mentioned systems are based on improved gas turbines for reaching the following targets: high efficiency (e.g. Humid Air Turbines or fuel cell based hybrid systems) and integration with renewable energy sources (e.g. externally fired gas turbines or machines including a solar system). However, considering biogas as fuel, all these advanced plant layouts will be essential for high efficient generation from renewable sources.

The main innovative aspect of this paper consists in the application of the proposed surge prevention technique based on a vibration precursor. Following the development of control system devices, the paper shows the technique demonstration in a real microturbine connected to a large

vessel size, as in the mentioned advanced plants. So, the application of this technique to a real plant including such additional volume (as in high-efficiency advanced cycles) produced innovative experimental results, as the first worldwide demonstration of the proposed control solution. Finally, a further innovative aspect included in this paper regards the application of this surge prevention technique to the compressor inlet temperature increase test. The demonstration carried out under this operative condition was important not only to show the technique flexibility, but also to focus special attention on risk operations, which are usually neglected in surge prevention devoted works.

2. Gas turbines with large volume components

Since in the advanced gas turbine layouts additional components are included between the compressor outlet and the expander inlet, a significant volume increase is obtained. This aspect is shown in Fig.1, where the components responsible for the significant volume increase are underlined. Although different layouts were proposed [28], these four systems could represent the main advanced cycles which significantly affect the gas turbine volume. Additional volume is also included for the recuperated and intercooled gas turbine cycles, but its size is not large enough to produce significant change in the dynamic behaviour.

Figure 1

Layout A in Fig.1 shows a general scheme for the externally fired gas turbines [29]. Although additional components can also be included, this scheme represents that the pressurized ducts of the furnace are responsible for the volume increase. However, in this case the volume increase could be similar to that related to the recuperated or intercooled gas turbines. So, risks associated with this component during the dynamic operation can be dependent on the component geometry.

Layout B in Fig.1 is reported as a general scheme of a Concentrated Solar Power (CSP) hybrid gas turbine system: CSP components are included between the compressor and the turbine [30]. Hybrid configuration can be considered to compensate the variability of solar input. However, in this case, the solar receiver components are significantly increasing the volume of gas turbine system, depending on the selected technology and the number of components. Although Fig.1 shows three modules, different configurations are possible with further modules including also heat exchangers (e.g. a recuperator).

Layout C in Fig.1 shows a Humid Air Turbine (HAT) power plant including an intercooler, an after-cooler and a recuperator (further components such as an economizer for water pre-heating can also be installed increasing the plant complexity) [10]. Even if these components are including an additional volume, the device which is responsible for the largest volume increase is the saturator [10]. This large vessel, which is essential for improving the performance, is responsible for dynamic behaviour unlike the standard cycle, and thus producing significant surge risks during the transient operations.

The plant type that includes the highest additional volume is the fuel cell based hybrid system [31]. Although layout D in Fig.1 shows a hybrid system based on a tubular Solid Oxide Fuel Cell (SOFC), where the air flow is pre-heated with a recuperator and the fuel system is based on an anodic ejector, different configurations are possible depending on the cell type and economic feasibility of the plant [32]. For this reason, plants with further recirculations or different components are possible (e.g. a cathodic recirculation instead of the recuperator). However, in all such cases, the large additional volume (mainly related to the fuel cell stack) is producing a different dynamic behaviour (including significant surge risk), in comparison with the standard turbines.

Another important notation needs to be included for gas turbines equipped with large volume systems to store the thermodynamic energy. In case of energy storage systems, based on the compressed air [33] or high temperature materials (e.g. honeycomb ceramics [34], thermo-chemical

reactors [35], etc.), a significant additional volume is included. In case of large vessels (e.g. thermal storage to compensate the variability of the solar source) the dynamic behaviour differs significantly from a standard machine. Due to the higher risk of surge, detection/prevention techniques have to be designed and implemented in the plant control system.

Figure 2

3. Test rig

The experimental activities presented in this paper were carried out with a T100 microturbine connected with external vessels, as shown in Fig.2. The nominal main properties of this recuperated turbine are: 100 kW electrical power, 30% electrical efficiency, and 70,000 rpm rotational speed. Since the turbine was modified for the external connections and the volume has resulted in significant temperature and pressure drop (99 K and 142 mbar, respectively), the T100 machine cannot achieve the nominal performance [36]. Hence, the test rig is able to produce 73.5 kW maximum net electrical power with compressor inlet temperature at 300 K and Turbine Outlet Temperature (TOT) at 918.15 K. The test rig, used for experiments on general advanced cycles presented in this paper, was originally designed for emulation of hybrid systems based on high temperature fuel cells [13]. For this reason, the external vessels include a modular unit for the cathodic side and a 0.8 m^3 device for the anodic side (also including a recirculation system based on an ejector). The total size of these vessels (including the connection pipes) is about 4.1 m^3 (0.1 m^3 volume size was not accounted in [13] because it was not included in the fuel cell emulator). However, to obtain an intermediate volume (considering the T100 size) generally representative of the advanced gas turbine systems, the modular vessel was arranged by removing three modules (Fig.3). So, the tests shown in this paper were carried out with 2.3 m^3 of additional volume. Moreover, to control the compressor inlet temperature (TC1 in Fig.2) three air/water heat

exchangers (called "Ex" in Fig.2) were installed. So, TC1 can be decreased/increased using open circuit water, an absorption chiller or a co-generation heat exchanger (see [13] for more details).

Figure 3

The facility shown in Fig.4 includes: a check valve installed downstream of the compressor outlet to minimize the risk of damage in case of surge events, turbine/vessel connection valves (VM and VO) for managing the air flow path and an emergency bleed valve (VBE). All the valve control systems and the installed measurement probes (in addition to the T100 standard instrumentation) were connected to an acquisition/control tool implemented in LabVIEW^{TM}. The location of the probes used in this work are reported in Fig.2, considering that more details on the measurement system and performance have been discussed in previous works, such as [13] for the anodic side and [14] for the microturbine and the modular vessel. In addition to the previously presented sensors [14], a tri-axial accelerometer (ACC in Fig.2) was installed on the top of the T100 generator case (x, y, z axes were oriented in the microturbine axial, tangential and radial direction, respectively) for investigating the frequency range up to 10 kHz [36].

Figure 4

While the LabVIEV™ control software (Fig.4) is operating on the additional probes installed in the connection pipes, the original turbine controller was maintained to ensure safe machine operation. Hence, similar to the standard T100 turbines in the grid-connected mode, the control system changes the fuel flow rate to maintain the TOT at its set-point (918.15 K). Although the main acquisition time step was fixed at 1 s, this value was 0.1 s for the PRC1, MR and the accelerometer. While the actual ACC acquisition frequency is significantly higher, 0.1 s is the time step used for the signal saving and control operations.

4. Surge prevention technique

Considering the trend of the RMS amplitude for the sub-synchronous vibration content (as shown in [36]), a surge prevention technique was developed and demonstrated with the T100 machine connected to the 2.3 m^3 vessel. This approach is simply based on a threshold calculation from the average RMS amplitude during operations far from surge and operation for surge avoidance in case exceeding the amplitude values. While a simple bleed valve opening was used in the tests to avoid surge, other operations (e.g. opening of bypass valves or smoothing transient operations with electrical batteries in case of fuel cell based plants) with similar effects can be considered in advanced systems.

In order to consider the influence of different operating conditions (e.g. the rotational speed change), instead of using a fixed value, the threshold was calculated as the average vibration RMS amplitude at normal operating conditions (far from the surge line) multiplied by 1.6. This multiplication factor was obtained from the previous experiments [36] and to maintain a good surge margin (Kp>1.1 considering the definition of Eq.1) during all operations. This margin was considered representative of advanced cycles where, in some cases, a surge event can be extremely dangerous for the components (e.g. for a fuel cell). In case of different volume sizes connected to the machine (as shown in [36] for this T100 microturbine), the same approach can be used even if

the average vibration RMS amplitude at normal operating conditions is different; the threshold value can be calculated by applying the same multiplication factor to a different reference value.

$$Kp = \frac{\beta_{sl} \cdot m}{\beta \cdot m_{sl}} \tag{1}$$

5. Experimental demonstration

Two different tests are presented to demonstrate this surge prevention technique. While the initial case is based on the surge approaching operation presented in [36] (increase of pressure losses in the pressurised zone), the demonstration is completed with the technique application to face possible risks due to compressor inlet temperature increase (TC1). Both tests were started with the T100 machine operating in grid-connected mode at net electrical power of 40 kW. The additional vessel was included in the loop (VO fully open and VM fully closed) and pre-heated up to the steady-state conditions.

5.1. Increase of pressure losses

For the test related to the increase of pressure losses the VO valve was gradually closed to generate an operating condition that was moving towards the surge line. This operation was similar to what has been reported in [36], where all the data were provided for both the steady-state and the surge approaching conditions. The compressor inlet temperature was maintained at 300 K, with cold water operating in the open loop condition.

Figure 5

The threshold crossing for the RMS amplitude value (calculated in real-time mode for the 5-800 Hz band) produced a change in the VBE control signal from "False" to "True", generating the opening step operation shown in Fig.5 (at time zero). Unlike the work presented in [36], where the

frequency range of 2-900 Hz was considered, in this work the band was reduced down to the 5-800 Hz to better highlight the property variation. Thanks to this bleed opening operation, the surge event was prevented and the vibration amplitude was reduced. Then, the surge cause was removed (at time 190 s in Fig.5) through re-opening the VO valve. While it is a simple solution for this demonstration activity, it represents different possible operations which can be carried out for advanced cycles, such as load change smoothing (with batteries or the electrical grid), bypass valve opening, generator motoring rates for the start-up/shutdown phases, etc. As soon as the surge cause was considered removed, the VBE was closed with a step (performed after 296 s from the surge risk detection) and a new steady-state condition was reached.

Figure 6

Figure 7

Further details related to this test are shown in Figs.6-8: the trends of recuperator inlet pressure (PRC1), rotational speed and net electrical power produced by the T100 turbine. As shown in [36], the VO closing generated significant pressure loss increase and, as a consequence, an increase in the PRC1 value. However, the increase in PRC1 (shown in Fig.6 before the VBE opening) is also significantly affected by the T100 rotational speed increase (Fig.7). This is managed by the T100 control system to pursue the load set-point that was fixed at 40 kW during the entire test. Since the VO closing direct effect decreased the generated net power (more power consumed by the compressor due to the increase in outlet pressure), the T100 control system managed the machine to increase the rotational speed and to align the turbine with its load set-point. This trend is also visible in the net power line reported in Fig.8. The VBE opening generated a significant decay of PRC1, thus preventing surge conditions. Moreover, Figs.7-8 show a decrease also in the rotational speed and the net electrical power. This is due to a threshold in the T100

power conditioning component: a constraint related to the voltage of the direct current bar that is implemented in the T100 control system. Hence, the air discharge due to the VBE opening produced an unbalanced condition reaching this voltage threshold. This resulted in net electrical power significantly lower than its set-point. Then, closing the VBE enabled to restore the requested net power condition.

Figure 8

Figure 9

To complete the test description, Fig.9 shows the operating line on the compressor map. While the initial and final points are almost superimposed, the VBE opening effect is significantly visible. After the initial path towards the surge line, the prevention technique was able to generate a trend almost parallel to this stability limit. This effect is also visible in the surge margin plot (Fig.10) calculated with Eq.1. While this parameter was decreasing before the VBE opening operation, the surge prevention technique was able to maintain a good margin (Kp>1.1), and thus avoiding any instability risk.

Figure 10

5.2. Compressor inlet temperature increase

For this test, the VO valve was maintained fixed at the 36% of its FO to operate in a region with a good surge margin, but affected with possible risks in case of further property changes. Then, the cooling water flow (for the TC1) was stopped leaving the TC1 to increase up to its uncooled conditions. The most significant part of this transient operation is shown in Figs.11 and 12: Figure 11 is mainly devoted to the vibration trend generated by the surge margin decrease due to the TC1

increase and Fig.12 shows the FO values of the involved valves. The vibration line is, in this case, the difference between the RMS value of the sub-synchronous content (5-800 Hz band) and the mentioned threshold. As soon as, the vibration values reached the threshold (zero in the right vertical axis of Fig.11), the control system activated the opening of the VBE valve (the dotted line in Fig.12) due to the mentioned control signal changed from "False" to "True". Also in this case the zero value of the time axis was fixed at the VBE valve opening.

Figure 11

Figure 12

Further details related to this test are shown in Figs.13-15: the trends of rotational speed, net electrical power produced by the T100 turbine and recuperator inlet pressure (PRC1). The compressor inlet temperature increase produced a significant decrease in the rotational speed and electrical power. As mentioned in the previous section, this is due to the threshold in the T100 power conditioning component: a constraint related to the voltage of the direct current bar that is implemented in the T100 control system. Moreover, the air discharge due to the VBE opening produced an unbalanced condition that generated a further rotational speed and power decrease. This resulted in a very low net electrical power (about 4.5 kW) at 150 s after the VBE opening. A similar trend due to both the rotational speed decrease and the air bleeding (after the VBE opening) is shown by the PRC1 plot (Fig.15).

Figure 13

Figure 14

Figure 15

To complete the test description, Fig.16 shows the operating line on the compressor map. In this case the rotational speed decrease generated a slight approaching trend towards the surge line. This produced the activation of the surge prevention technique and the consequent VBE opening. This technique was able to generate a slight trend modification avoiding any risk due to the TC1 increase. This effect is also visible in the surge margin plot (Fig.17 shows a detail related to the prevention technique activation) calculated with Eq.1. While this parameter was decreasing before the VBE opening operation, the surge prevention technique was able to maintain a good margin (Kp>1.1), and thus avoiding any instability risk also for this case (TC1 increase).

Figure 16

Figure 17

6. Details on possible real applications

The obvious application of this demonstrated surge prevention technique is related to gas turbines connected to large volume components. So, the implementation of this approach is a promising solution to enlarge the operative field of these systems, such as fuel cell based plants, micro Humid Air Turbine (micro-HAT) systems, and externally fired microturbines (including CSP applications). The main impact will regard mainly flexibility, efficiency increase in part-load operations and gas turbines fed by renewable sources (CSP or biogas) [37]. Moreover, important benefits will involve also systems under research or improvement (i.e. SOFC-based hybrid systems [38]), enlarging the market penetration opportunities. Moreover, since this technique is based on

standard low cost components, the application in commercial systems will not affect significantly the energy price [39].

Although the paper results were obtained with a microturbine (due to the interest in such plants for distributed generation), the technique is a general approach available also for large size machines with standard components (if necessary for the related application). As shown by the results presented in this paper, vibration measurement during standard operative conditions will be enough for setting the algorithm. However, different multiplication factors can be applied (e.g. a scheduling table taking into account different operative conditions could be included) depending on the specific surge margin value that is considered acceptable for the application.

The results obtained for the compressor inlet temperature increase (representative of critical operations of both microturbines and large size machines) highlight the importance of considering the influence of ambient conditions. So, the application of this flexible surge prevention technique will be essential also for avoiding risks due to these operations.

7. Conclusions

This paper shows the experimental results obtained from a facility based on a recuperated microturbine, to demonstrate a surge prevention technique for the turbine-based advanced power plants. This research activity is a significant improvement for advanced plants affected by the surge risks (especially during transient operations) due to a large volume size installed between the compressor outlet and the turbine inlet. The main conclusions derived from this work are summarized in the following points:

- identification of the vibration root-mean-square amplitude in a sub-synchronous band (5-800 Hz) as a real-time parameter, that is able to show the approaching of surge events;
- implementation of the prevention/recovery technique on the basis of a vibration threshold, which is evaluated from the average value during the standard conditions;

- threshold calculation able to compensate the variation of operative conditions (e.g. the rotational speed);
- demonstration of the surge prevention technique (with the control system operating on the emergency bleed valve) maintaining a good surge margin (higher than 1.1) during two different tests (increase in pressure losses and compressor inlet temperature).
- especially the test related to the compressor inlet temperature increase demonstrated a good flexibility of the surge prevention technique also for operations different from what is usually investigated (surge risk is usually analysed in case of pressure increase between the compressor and the turbine, while other operations linked with such similar risk are not usually fully considered).

Although the positive results obtained in this work, ongoing activities are under development by the Thermochemical Power Group to consider further surge precursor parameters and their application in the turbine control systems.

Acknowledgements

The authors would like to thank Dr. Matteo Pascenti, laboratory technician at TPG, for his essential activity in the test preparation and management.

The test rig was partially funded by (i) FP6 and FP7 EU projects, (ii) National projects, and (iii) Rolls-Royce Fuel Cell Systems.

Nomenclature

Variables

FO	Fractional Opening [%]
Kp	surge margin [-]
m	mass flow rate [kg/s]

N	rotational speed [rpm]
TOT	Turbine Outlet Temperature [K]
β	pressure ratio [-]

Subscripts

0	design
sl	surge limit on compressor map

Acronyms

CSP	Concentrated Solar Power
E. grid	Electrical grid
Ex	heat Exchanger
HAT	Humid Air Turbine
REC	RECuperator
RMS	Root Mean Square
SOFC	Solid Oxide Fuel Cell
TPG	Thermochemical Power Group

References

[1] Sheikhbeigi B., Ghofrani, M.B,. Thermodynamic and environmental consideration of advanced gas turbine cycles with reheat and recuperator. International Journal of Environmental Science and Technology, 4 (2007) 253-262.

[2] Locatelli M., Contribution of gas turbines to energy savings with high efficiency systems. Applied Energy, 36 (1990) 89-92.

[3] Traverso, A., Massardo, A.F., Thermoeconomic analysis of mixed gas-steam cycles. Applied Thermal Engineering, 22 (2002) 1-21.

[4] Jana K., Ray A., Majoumerd M.M., Assadi M., De S., Polygeneration as a future sustainable energy solution – A comprehensive review. Applied Energy, 202 (2017) 88-111.

[5] Yan J., Chou S.K., Desideri U., Xia X., Innovative and sustainable solutions of clean energy technologies and policies (Part I). Applied Energy, 130 (2014) 447-449.

[6] McDonald C.F., Massardo A.F., Rodgers C., Stone A., Recuperated gas turbine aeroengines, part I: Early development activities. Aircraft Engineering and Aerospace Technology, 80 (2008) 139-157.

[7] Al-Sharafi A., Yilbas B.S., Sahin A.Z., Ayar T., Performance assessment of hybrid power generation systems: Economic and environmental impacts. Energy Conversion and Management, 132 (2017) 418-431.

[8] Henke M., Monz T., Aigner M., Introduction of a New Numerical Simulation Tool to Analyze Micro Gas Turbine Cycle Dynamics. Journal of Engineering for Gas Turbine and Power, 139 (2017) 042601_1-7.

[9] Qiu K., Yan L., Ni M., Wang C., Xiao G., Luo, Z., Cen, K., Simulation and experimental study of an air tubecavity solar receiver. Energy Conversion and Management, 103 (2015) 847-858.

[10] Montero Carrero M., De Paepe W., Parente A., Contino F., T100 mGT converted into mHAT for domestic applications: Economic analysis based on hourly demand. Applied Energy, 164 (2016) 1019-1027.

[11] Pedemonte A.A., Traverso A., Massardo A.F., Experimental analysis of pressurised humidification tower for humid air gas turbine cycles. Part A: Experimental campaign. Applied Thermal Engineering, 28 (2008) 1711-1725.

[12] Zaccaria V., Tucker D., Traverso A., Transfer function development for SOFC/GT hybrid systems control using cold air bypass. Applied Energy, 165 (2016) 695-706.

[13] Ferrari M.L., Pascenti M., Magistri L., Massardo A.F., MGT/HTFC hybrid system emulator test rig: Experimental investigation on the anodic recirculation system. Journal of Fuel Cell Science and Technology, 8 (2011) 021012_1-9.

[14] Ferrari M.L., Pascenti M., Magistri L., Massardo A.F., Hybrid system test rig: Start-up and shutdown physical emulation. Journal of Fuel Cell Science and Technology, 7 (2010) 021005_1-7.

[15] McLarty D., Brouwer J., Samuelsen S., Fuel cell-gas turbine hybrid system design part II: Dynamics and control. Journal of Power Sources, 254 (2014) 126-136.

[16] Liškiewicz G., Horodko L., Time-frequency analysis of the Surge Onset in the Centrifugal Blower. Open Engineering, 5 (2015) 299-306.

[17] Zaccaria V., Tucker D., Traverso A., Operating strategies to minimize degradation in fuel cell gas turbine hybrids. Applied Energy, 192 (2017) 437-445.

[18] Fanyu L., Jun L., Stall Warning Approach With Application to Stall Precursor-Suppressed Casing Treatment. ASME Paper GT2016-58172, ASME Turbo Expo 2016, Seoul, South Korea.

[19] Morini M., Pinelli M., Venturini M., Acoustic and Vibrational Analyses on a Multi-Stage Compressor for Unstable Behavior Precursor Identification. ASME Paper GT2007-27040, ASME Turbo Expo 2007, Montreal, Canada.

[20] Zaccaria V., Tucker D., Traverso A., Transfer function development for SOFC/GT hybrid systems control using cold air bypass, Applied Energy, 165 (2016) 695-706.

[21] Caratozzolo F., Ferrari M.L., Traverso A., Massardo A.F., Emulator rig for SOFC hybrid systems: Temperature and power control with a real-time software. Fuel Cells, 13 (2013) 1123-1130.

[22] Gopisetty S., Treffinger P., Reindl L.M., Open-source energy planning tool with easy-to-parameterize components for the conception of polygeneration systems. Energy, 126 (2017) 756-765.

[23] Ferrari M.L., Traverso A., Massardo A.F., Smart polygeneration grids: Experimental performance curves of different prime movers. Applied Energy, 162 (2016) 622-630.

[24] Kang, S., Ahn, K.-Y., Dynamic modeling of solid oxide fuel cell and engine hybrid system for distributed power generation. Applied Energy 195 (2017) 1086-1099.

[25] Hagino N., Uda K., Kashiwabara Y., Prediction and Active Control of Surge Inception of a Centrifugal Compressor. Proceedings of the International Gas Turbine Congress, 2003.

[26] Arnulfi G.L., Giannattasio P., Giusto C., Massardo A.F., Micheli D., Pinamonti P., Multistage Centrifugal Compressor Surge Analysis. Part I: Experimental Investigation, Journal of Turbomachinery. 121 (1999) 305-311.

[27] Arnulfi G.L., Giannattasio P., Giusto C., Massardo A.F., Micheli D., Pinamonti P., Multistage centrifugal compressor surge analysis: Part II-numerical simulation and dynamic control parameters evaluation. Journal of Turbomachinery, 121 (1999) 312-320.

[28] Fallah M., Siyahi H., Ghiasi R.A., Mahmoudi S.M.S., Yari M., Rosen M.A., Comparison of different gas turbine cycles and advanced exergy analysis of the most effective. Energy 116 (2016) 701-715.

[29] Al-attab K.A., Zainal Z.A., Externally fired gas turbine technology: A review. Applied Energy, 138 (2015) 474-487.

[30] Mokheimer E.M.A., Dabwan Y.N., Habib M.A., Optimal integration of solar energy with fossil fuel gas turbine cogeneration plants using three different CSP technologies in Saudi Arabia. Applied Energy, 185 (2017) 1268-1280.

[31] Ferrari M.L., Massardo A.F., Cathode–anode side interaction in SOFC hybrid systems. Applied Energy, 105 (2013) 369–379.

[32] Otomo, J., Oishi, J., Miyazaki, K., Okamura, S., Yamada, K. Coupled analysis of performance and costs of segmented-in-series tubular solid oxide fuel cell for combined cycle system. International Journal of Hydrogen Energy, 42 (2017) 19190-1920.

[33] Sun H., Luo X., Wang J., Feasibility study of a hybrid wind turbine system - Integration with compressed air energy storage. Applied Energy, 137 (2015) 617-628.

[34] Mahmood M., Traverso A., Traverso A.N., Massardo A.F., Marsano D., Cravero C., Thermal energy storage for CSP hybrid gas turbine systems: Dynamic modelling and experimental validation. Applied Energy, 212 (2018) 1240-1251.

[35] Aydin D., Casey S.P., Riffat S., The latest advancements on thermochemical heat storage systems. Renewable and Sustainable Energy Reviews, 41 (2015) 356-367.

[36] Ferrari M.L., Silvestri P., Pascenti M., Reggio F., Massardo A.F., Experimental Dynamic Analysis on a T100 Microturbine Connected With Different Volume Sizes. Journal of Engineering for Gas Turbines and Power, 140 (2018) 021701_1-12.

[37] Yuan R., Rodrigues J.F.D., Tukker A., Behrens P., The impact of the expansion in non-fossil electricity infrastructure on China's carbon emissions. Applied Energy, 228 (2018) pp.1994-2008.

[38] Azizi M.A., Brouwer J., Progress in solid oxide fuel cell-gas turbine hybrid power systems: System design and analysis, transient operation, controls and optimization. Applied Energy, 215 (2018) 237-289.

[39] Hensher, D.A., Shore, N., Train, K. Willingness to pay for residential electricity supply quality and reliability. Applied Energy, 115 (2014) 280-292.

Figures

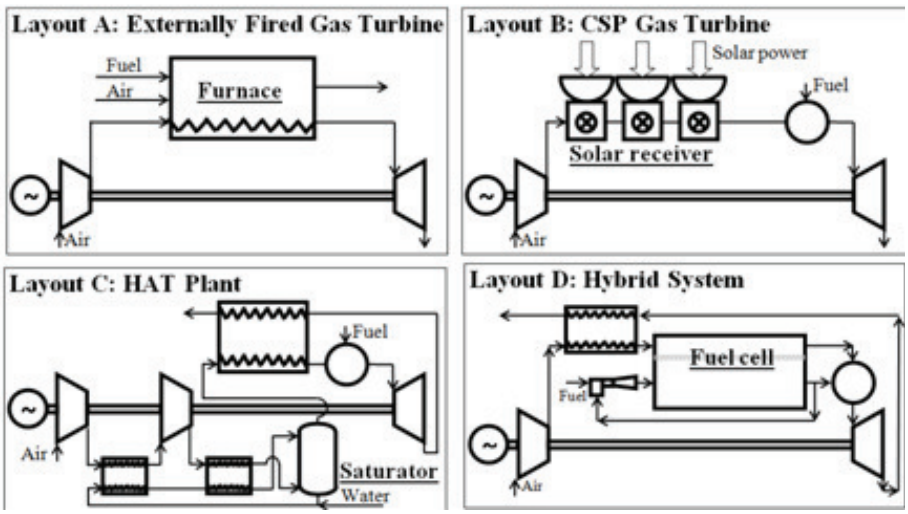

Figure 1. Main gas turbine advanced layouts.

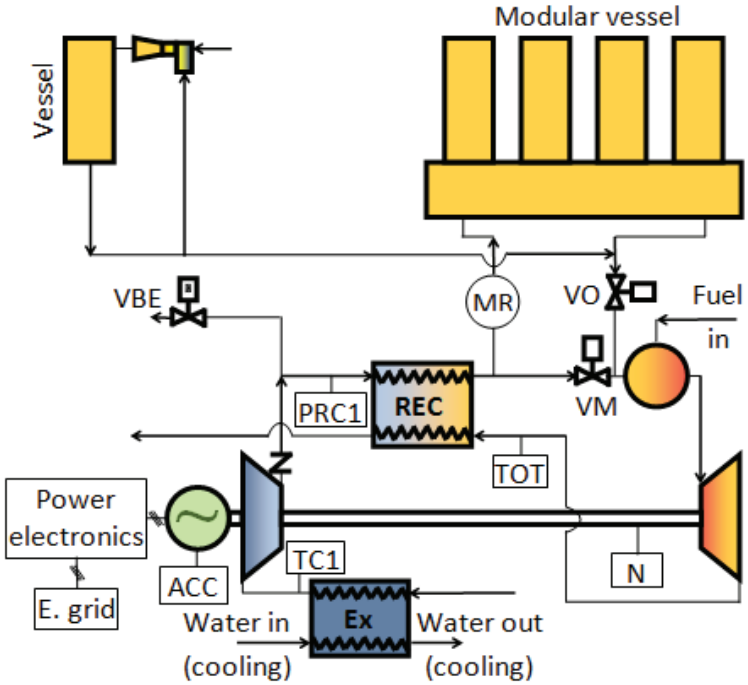

Figure 2. Test rig layout.

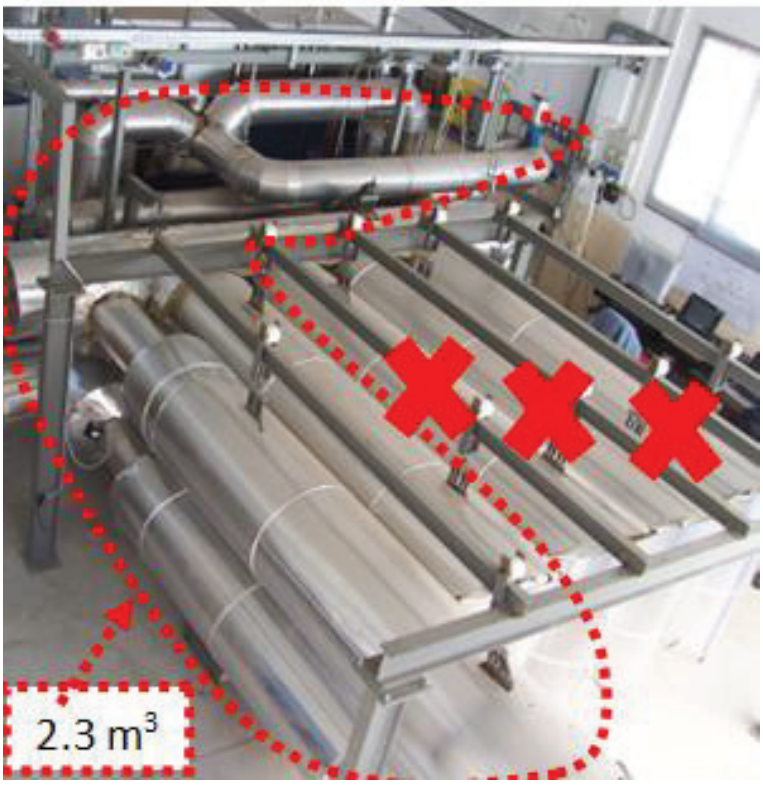

Figure 3. Test rig picture.

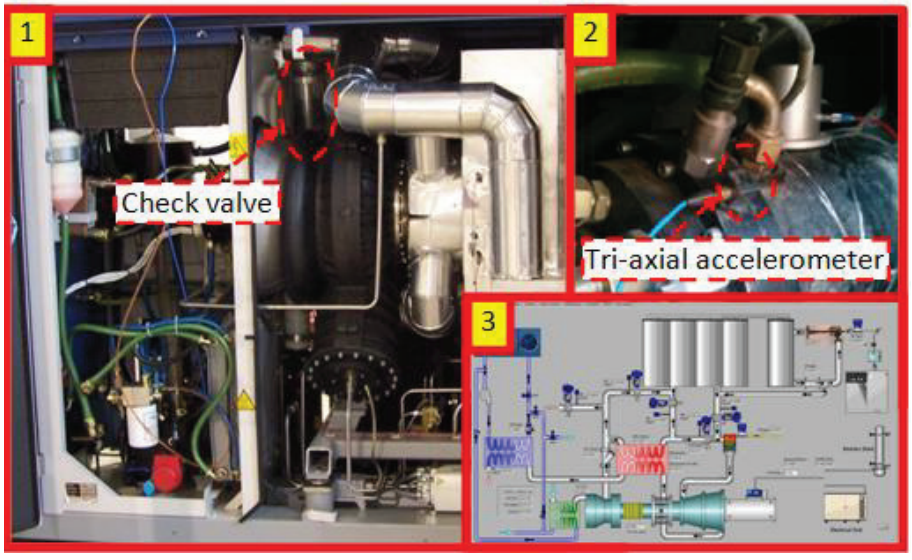

Figure 4. Test rig details: (1) T100 power module, (2) tri-axial accelerometer location, (3) LabVIEV™ control software (front panel).

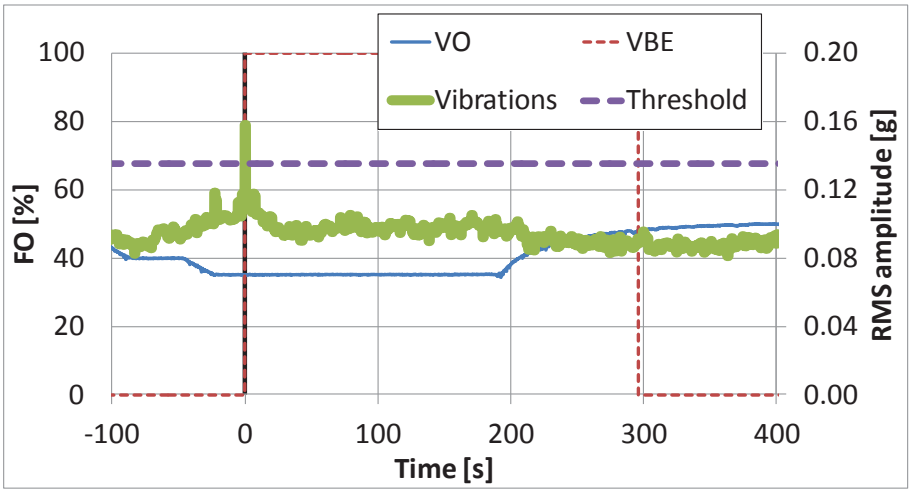

Figure 5. Experimental demonstration for the increase of pressure losses: valve FO values and RMS amplitude value for the 5-800 Hz band.

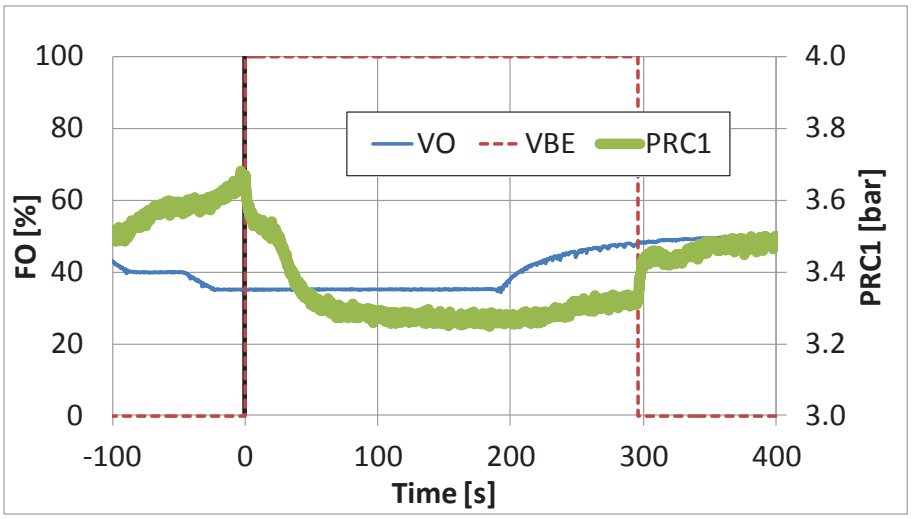

Figure 6. Experimental demonstration for the increase of pressure losses: valve FO values and recuperator inlet pressure.

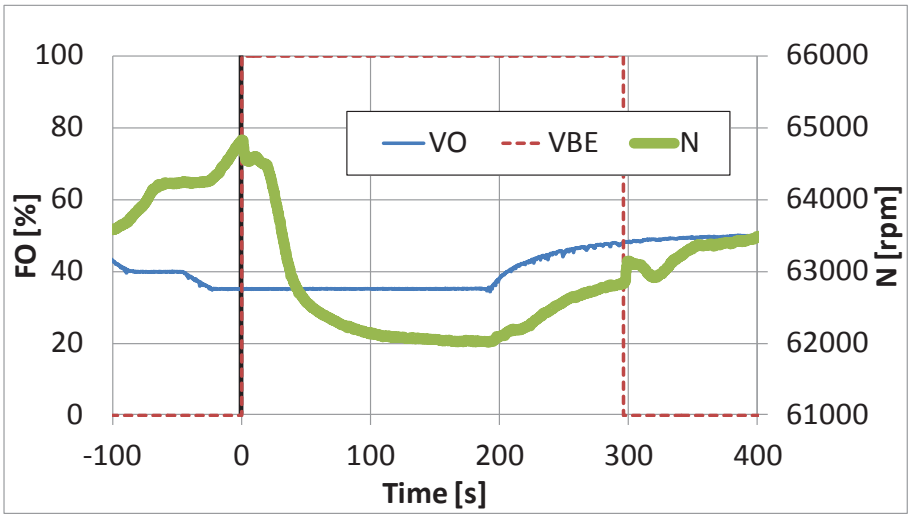

Figure 7. Experimental demonstration for the increase of pressure losses: valve FO values and T100 rotational speed.

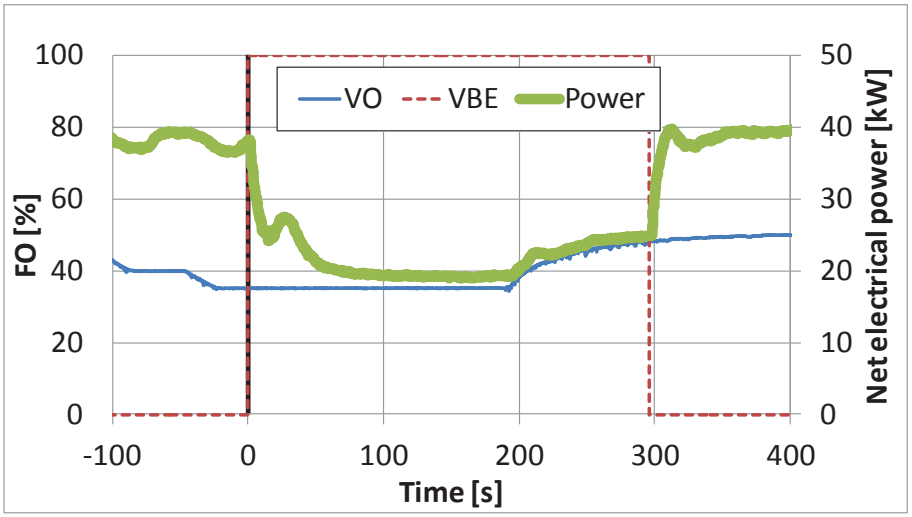

Figure 8. Experimental demonstration for the increase of pressure losses: valve FO values and T100 net electrical power.

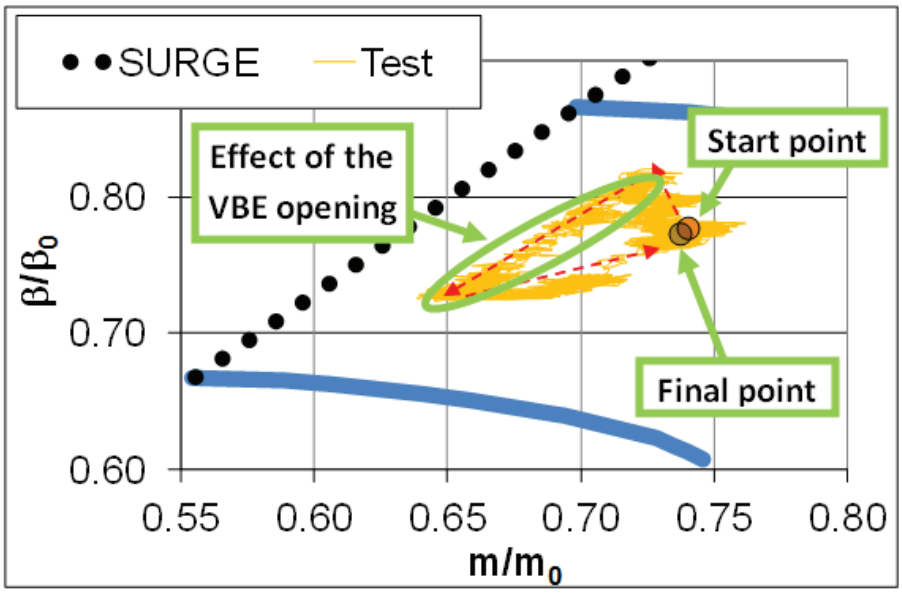

Figure 9. Experimental demonstration for the increase of pressure losses: the test on the compressor map.

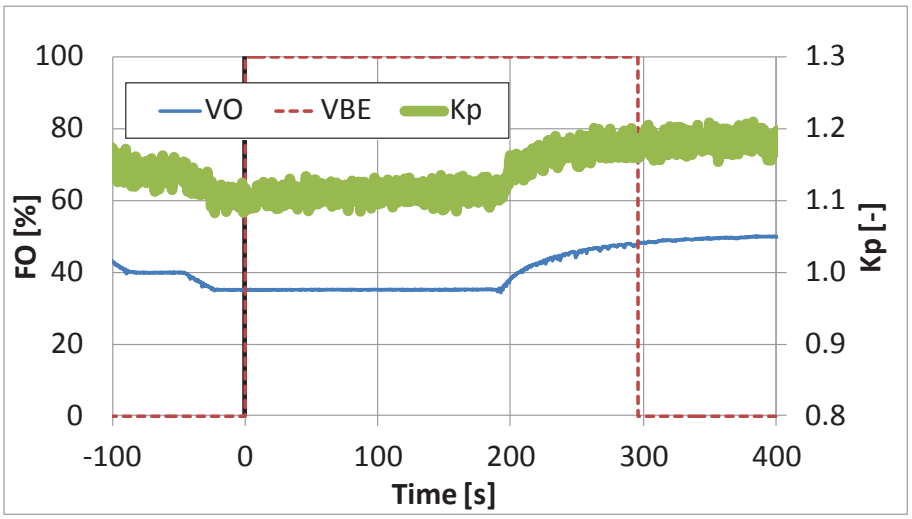

Figure 10. Experimental demonstration for the increase of pressure losses: surge margin.

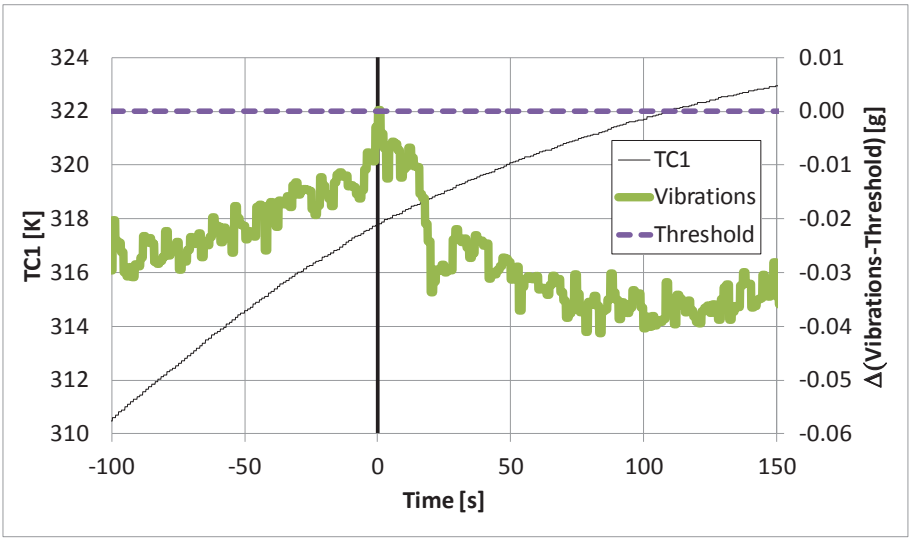

Figure 11. Experimental demonstration for the compressor inlet temperature increase: TC1 and vibration values (difference between the RMS amplitude value for the 5-800 Hz band and the threshold).

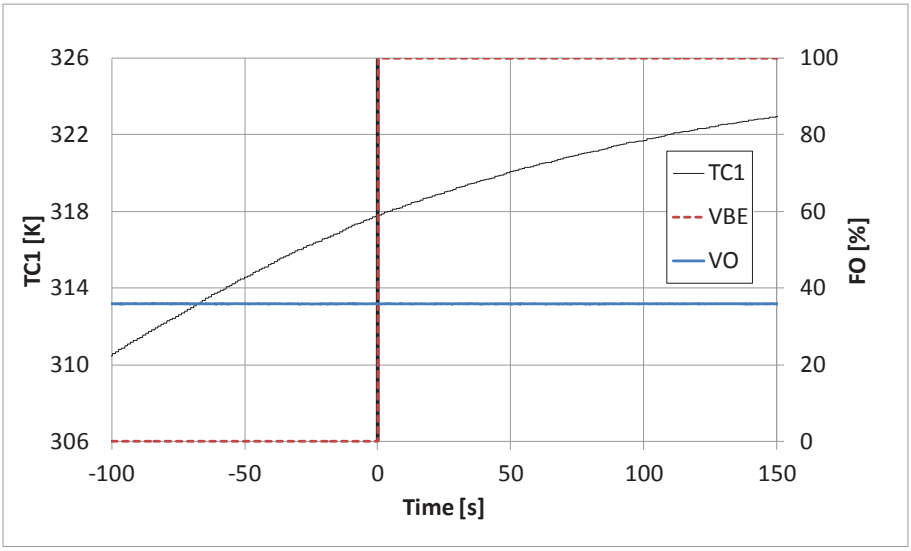

Figure 12. Experimental demonstration for the compressor inlet temperature increase: TC1 and valve fractional opening values.

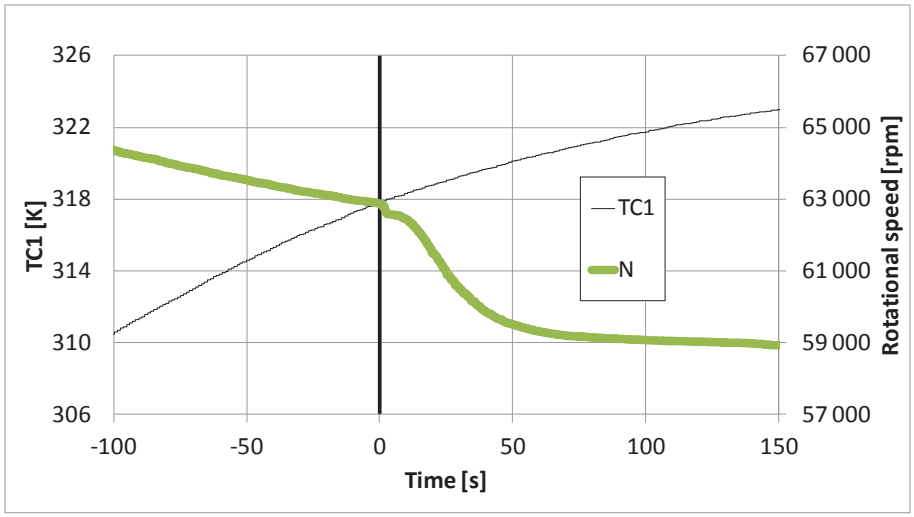

Figure 13. Experimental demonstration for the compressor inlet temperature increase: TC1 and rotational speed.

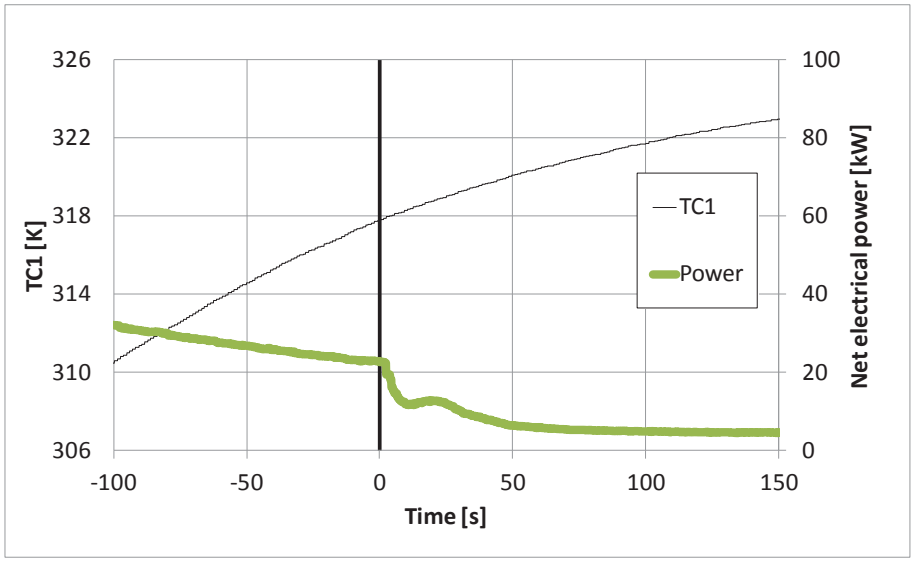

Figure 14. Experimental demonstration for the compressor inlet temperature increase: TC1 and net electrical power.

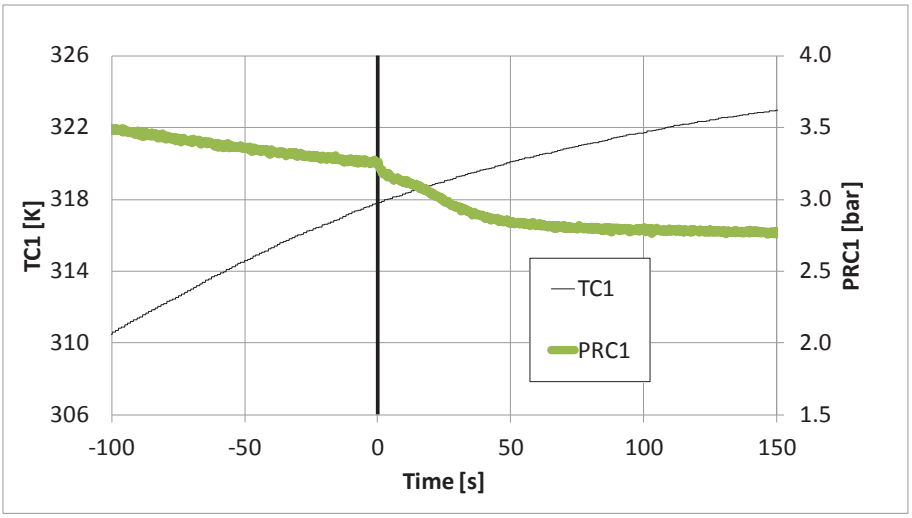

Figure 15. Experimental demonstration for the compressor inlet temperature increase: TC1 and recuperator inlet pressure.

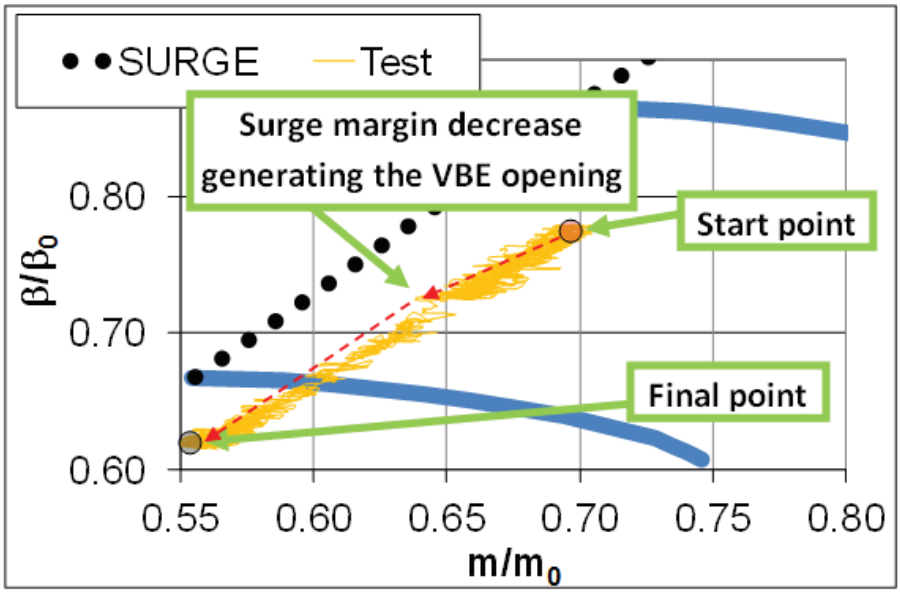

Figure 16. Experimental demonstration for the compressor inlet temperature increase: the test on the compressor map.

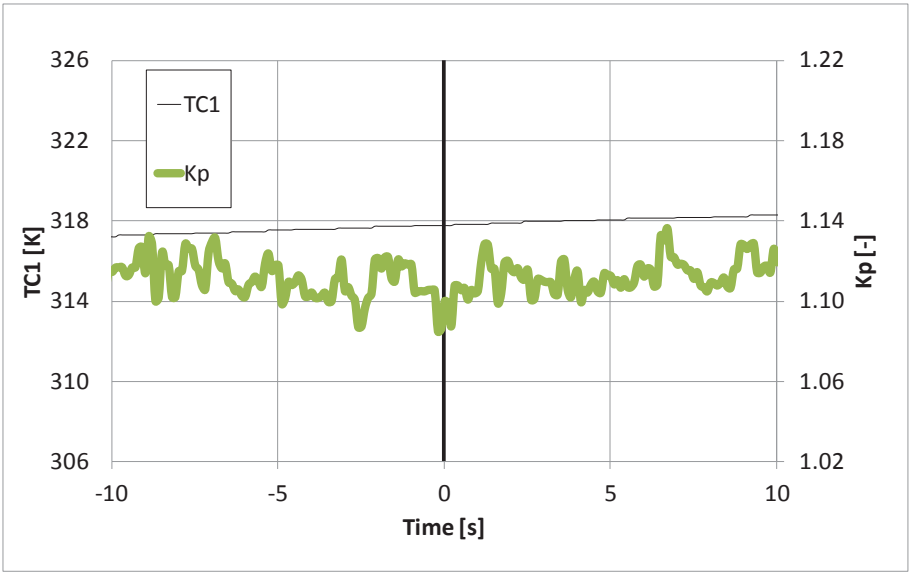

Figure 17. Experimental demonstration for the compressor inlet temperature increase: detail of the surge margin trend.